Structural Determinants for Inhibitor Specificity and Selectivity in PDE2A Using the Wheat Germ in Vitro Translation System†

André Iffland,‡,§ Darcy Kohls,‡ Simon Low,‡ Jing Luan,‡ Yan Zhang,‡ Michael Kothe,‡ Qing Cao,‡ Ajith V. Kamath,‡ Yuan-Hua Ding,*,‡ and Tom Ellenberger*,§,||

Department of Biology, Pfizer Research Technology Center, Cambridge, Massachusetts 02139, and Department of Biological Chemistry and Molecular Pharmacology, Harvard Medical School, Boston, Massachusetts 02115

Received December 21, 2004; Revised Manuscript Received April 20, 2005

ABSTRACT: Phosphodiesterases (PDEs) modulate signaling by cyclic nucleotides in diverse processes such as cardiac contractility, platelet aggregation, lipolysis, glycogenolysis, and smooth muscle contraction. Cyclic guanosine monophosphate (cGMP) stimulated human phosphodiesterase 2 (PDE2) is expressed mainly in brain and heart tissues. PDE2A is involved in the regulation of blood pressure and fluid homeostasis by the atrial natriuretic peptide (ANP), making PDE2-type enzymes important targets for drug discovery. The design of more potent and selective inhibitors of PDE2A for the treatment of heart disease would be greatly aided by the identification of active site residues in PDE2A that determine substrate and inhibitor selectivity. The identification of active site residues through traditional mutational studies involves the time-consuming and tedious purification of a large number of mutant proteins from overexpressing cells. Here we report an alternative approach to rapidly produce active site mutants of human PDE2A and identify their enzymatic properties using a wheat germ in vitro translation (IVT, also known as cell-free translation) system. We also present the crystal structure of the catalytic domain of human PDE2A determined at 1.7 Å resolution, which provided a framework for the rational design of active site mutants. Using a rapid IVT approach for expression of human PDE2A mutants, we identified the roles of active site residues Asp811, Gln812, Ile826, and Tyr827 in inhibitor and substrate selectivity for PDE2A.

Cyclic nucleotide second messengers (cAMP[1] and cGMP) play central roles in signaling pathways that regulate physiological responses. Cellular responses to these signals occur within a narrow concentration range of cAMP and cGMP, requiring precise control of the intracellular levels of these second messengers (*1*, *2*) by cyclic nucleotide synthetases and phosphodiesterases (PDE). Cyclic nucleotide phosphodiesterases (PDEs) comprise a large family of metallophosphohydrolases (e.g., Mg^{2+} and Zn^{2+}) that cleave the 3′,5′-cyclic phosphate moiety of cAMP and/or cGMP to produce the corresponding 5′ nucleoside monophosphate (*3*), thereby terminating the cyclic nucleotide signal. PDEs modulate cellular levels of cAMP and/or cGMP in processes such as cardiac contractility, platelet aggregation, lipolysis, glycogenolysis, smooth muscle contraction, ion channel conductance, and apoptosis (*3*, *4*).

The 21 PDEs in mammals can be subdivided into 11 families named PDE1 to PDE11. Although the members of each PDE family show a considerable divergence of amino acid sequences, they are functionally related according to their substrate and inhibitor specificities and the mechanism(s) of regulating enzymatic activity. The PDE5, PDE6, and PDE9 enzymes utilize cGMP as substrate, PDE4, PDE7, and PDE8 are specific for cAMP, and PDE1, PDE2, PDE3, PDE10, and PDE11 degrade both substrates. Functional analyses and amino acid sequence comparisons of various PDEs indicate that all PDEs are multidomain proteins with different domains functioning in catalysis and the regulation of activity. The amino acid sequences of all mammalian PDEs identified to date include a highly conserved C-terminal region of approximately 270 amino acids that encompasses the active site (*5*). The catalytic sites of the cAMP and/or cGMP PDEs include two putative metal (presumably zinc) binding sites as well as family-specific features of substrate and inhibitor specificity (*3*, *6*). The amino-terminal regions of PDEs are highly variable and include family-specific determinants, including (I) calmodulin binding sites (PDE1); (II) noncatalytic cGMP binding sites

† This work was supported by Pfizer Inc. and a research grant from Pfizer Inc. to Harvard Medical School.

* To whom correspondence should be addressed. T.E.: Department of Biological Chemistry and Molecular Pharmacology, Harvard Medical School, 240 Longwood Avenue, Boston, MA 02115-5730. Tel: 617-432-0458. Fax: 617-432-3380. E-mail: tome@hms.harvard.edu. Y.-H.D.: Department of Biology, Pfizer Research Technology Center, 620 Memorial Drive, Cambridge, MA 02139. Tel: 617-551-3168. Fax: 617-551-3178. E-mail: yuan-hua_ding@cambridge.pfizer.com.

‡ Pfizer Research Technology Center.

§ Harvard Medical School.

|| The Hsien Wu and Daisy Yen Wu Professor of Biological Chemistry and Molecular Pharmacology.

[1] Abbreviations: IVT, in vitro translation; EHNA, *erythro*-9-(2-hydroxy-3-nonyl)adenine; cAMP, cyclic adenosine monophosphate; CNS, central nervous system, cGMP, cyclic guanosine monophosphate; DMSO, dimethyl sulfoxide; PDE, phosphodiesterase; ATP, adenosine triphosphate; ANP, atrial natriuretic peptide; HEPES, *N*-2-hydroxyethylpiperazine-*N*′-2-ethane sulfonic acid; tRNA, transfer RNA; TCEP, tris(2-carboxyethyl)phosphine; PMSF, phenylmethanesulfonyl fluoride; MOI, multiplicity of infection; β-ME, β-mercaptoethanol; RMSD, root square mean distance; RT, room temperature.

10.1021/bi047313h CCC: $30.25
Published on Web 05/17/2005

(PDE2, PDE5, PDE6); (III) membrane targeting sites (PDE4); (IV) hydrophobic membrane association sites (PDE3); and (V) phosphorylation sites for either the calmodulin-dependent kinase (II) (PDE2), the cAMP-dependent kinase (PDE1, PDE3, PDE4), or the cGMP dependent-kinase (PDE5) (*3*, *7*).

Members of the PDE superfamily also differ substantially in their tissue distributions and expression levels, making them interesting therapeutic targets for a variety of diseases. It is of great pharmaceutical interest to understand the biological meaning of this apparent complexity by developing specific inhibitors of various PDEs that can be used to evaluate their physiological functions in animal models. For example, PDE5 is one of the several PDEs degrading cGMP in corpus carvernosum tissue (*8*). PDE5-specific inhibitors such as sildenafil (Viagra, $IC_{50} \sim 3.5$ nM), vardenafil (Levitra, IC_{50} 0.7 nM), and tadalafil (Cialis, IC_{50} 0.94 nM) lead to prolonged smooth muscle relaxant effects, confirming that the NO-cGMP pathway in corpus cavernosum vascular smooth muscle cells is predominately mediated by PDE5. These inhibitors are now marketed as drugs for male erectile dysfunction (*9*). Furthermore, design of specific inhibitors is also of great importance because the lack of specificity could cause undesirable side effects through inhibition of other PDEs.

Members of the PDE2 family function in cardiac Ca^{2+} channel control and ANP stimulation, which regulates blood pressure and fluid homeostasis. PDE2 is highly expressed in the brain and heart, but it is also found in lung, kidney, and liver (*10*). Full length human PDE2A possesses two N-terminal GAF domains (named for their presence in cGMP-regulated PDE, adenylyl cyclases, and the *Escherichia coli* protein Fh1A) in addition to the C-terminal catalytic domain (*11*, *12*)). The first GAF domain promotes dimerization of PDE2A, and the second GAF domain allosterically regulates catalytic activity in response to cGMP (*11*). Full-length PDE2A can hydrolyze both cAMP and cGMP, with a slightly lower apparent K_m for cGMP. However, when cGMP binds to the allosteric GAF domain, the enzyme undergoes a conformational change that results in a 10-fold lower K_m for cAMP.

PDE2A is selectively inhibited by EHNA (*erythro*-9-(2-hydroxy-3-nonyl)adenine) with an IC_{50} value of 1 μM (*3*). EHNA is the only PDE2-specific inhibitor that is commercially available. Other inhibitors, like the PDE4-specific inhibitor rolipram (IC_{50} 0.31 μM for PDE4) (*13*), possess IC_{50} values of 50 to 200 μM and do not significantly inhibit PDE2 (*14*−*18*). An inhibitor of PDE2A that is more potent and selective than EHNA would be useful for identifying the biological functions in various tissues and understanding the disease relevance of this enzyme (*19*). A better understanding of the specificity determinants within the PDE2A active site would greatly facilitate the design of potent PDE2A inhibitors. However, generation of large numbers of potential active site mutations and the production and characterization of these mutant proteins by conventional methods would make this a tremendously time-consuming effort.

In the present study, site directed mutagenesis was used in combination with an in vitro wheat germ protein translation system to rapidly identify key residues of human PDE2A that are important for the different inhibitory potencies of EHNA and rolipram. We also report a three-dimensional structure of the catalytic domain of hPDE2A determined at a resolution of 1.7 Å. A comparison of the human PDE2A crystal structure with the structure of PDE4D in complex with rolipram (*20*) suggested key residues that might be responsible for the selective inhibition of PDE2A. Fourteen residues were mutated singly or in different combinations, and the mutant proteins were expressed in a wheat germ extract based IVT system. The His_6-tagged mutant proteins were partially purified by affinity capture, and their kinetic parameters were measured and compared with those of the wild-type protein. Several mutations affected inhibition by rolipram and EHNA, and these residues are implicated as specificity determinants of inhibitor potency. Our results suggest that the IVT system is a convenient method to rapidly generate proteins for mutational studies of their enzymatic activities. The crystal structure of PDE2A and the models for binding of inhibitors EHNA and rolipram and both substrates in the active site may not only elucidate the role of amino acids important for inhibitor selectivity but also determine residues important for substrate specificity.

EXPERIMENTAL PROCEDURES

Wheat Germ Extract. Wheat germ was obtained from Baystate Milling Company, Clifton, NJ. All procedures were performed at 4 °C unless otherwise stated. Typically 60 g of wheat germ was frozen in liquid nitrogen and ground in a mortar to fine powder with an equal amount of acid washed sand. The powder was mixed with 120 mL of extraction buffer (20 mM HEPES, 100 mM potassium acetate, 1 mM magnesium acetate, 6 mM β-mercaptoethanol (β-ME), pH 7.5), incubated for 2 min, and centrifuged at 30000*g* for 10 min. The middle layer was carefully removed from the supernatant and centrifuged again at 30000*g* for 10 min. A buffer exchange (20 mM HEPES, 120 mM potassium acetate, 1 mM magnesium acetate, 6 mM β-ME, pH 7.2) was performed on a Sephadex G25 column, and wheat germ extract fractions were collected. The most active fractions (two-thirds of the extract) were pooled and stored at −80 °C. The average yield of crude wheat germ extract was 40 mL. The quality of each batch of wheat germ extract was compared to the quality of a reference batch by in vitro translation with a standard ^{35}S-Met radiolabled protein using band densitometry. Extract optimization was done to obtain the highest yield for each batch by adjusting β-ME, magnesium, and potassium ion concentrations.

In Vitro Translation Reaction and Affinity Capture of Proteins. The in vitro translation reaction mixture contained 20 mM HEPES, 1 mM ATP, 83 μg/mL creatine phosphokinase, 8.4 mM creatine phosphate, 21 μM GTP, 0.625 mM spermidine, 1.2 mM magnesium acetate, 10.5 μg/mL tRNA from wheat germ, 78.1 mM potassium acetate, 26 μM amino acid mixture, 2.1 mM β-ME, and 25% wheat germ extract. No RNase or protease inhibitors were added. Protein translation was performed at 28 °C and pH 7.2 for 1 h after the addition of 6.8 μg of capped mRNA. The mixture was then cooled to 4 °C, and 5 μL of a standardized Pharmacia nickel-chelating Sepharose suspension in 40 μL of assay buffer (100 mM Tris-HCl, 5 mM magnesium chloride, 2 mM β-ME, pH 7.5) was added to the translation mixture and incubated with slow shaking for 90 min to allow binding of the His_6-tagged proteins. Beads were collected by centrifuga-

tion, transferred to a clean tube, washed with assay buffer to remove endogenous unbound proteins, and stored on ice.

Phosphodiesterase Activity Assay. Phosphodiesterase activity was assayed by the $ZnSO_4/Ba(OH)_2$ precipitation method of Schilling et al. (*21*) in 96-well filter plates (Millipore, MHVBN4510) with modifications. The enzyme produced by in vitro translation was immobilized on Ni^{2+}-NTA resin and then incubated in assay buffer at 22 °C, with either cGMP (Sigma-Aldrich)/[8-^{3}H]cGMP (Amersham, TRK392) or cAMP (Sigma-Aldrich)/[2,8-^{3}H]cAMP (Amersham, TRK498) as substrate. The enzyme beads were mixed continuously during the assay. Sample aliquots were taken at the indicated times, quenched in a solution of 5.4 mM $ZnSO_4$, and then precipitated with 4.4 mM of $Ba(OH)_2$ for 45 min. The plates were washed (Brandel, Microdispenser XRM) with 1 mL of wash buffer (1 mM NaOH, 100 mM NaCl) per well and dried for 25 min on both sides under a heat lamp. Following the addition of 40 μL of scintillation fluid (Perkin-Elmer, Optiphase Supermix) per well, plates were read out on a Wallac Microbeta Trilux microplate liquid scintillation counter. K_m determinations for PDE2A were done at cGMP concentrations varying between 1 μM and 100 μM and for cAMP between 2.5 μM and 100 μM. K_m and V_{max} values were obtained from direct plots of the linear initial velocity v_0 (total substrate conversion < 10%) versus the substrate concentration S and are the result of triplicate measurements of at least two independent enzyme preparations. k_{cat} values were determined by dividing V_{max} by the molar concentration of enzyme, estimated as described below. IC_{50} values were measured at substrate concentrations of 1/10 of the K_m value with inhibitor concentrations varying from 1 μM to 3 mM for rolipram and 10 nM to 30 μM for EHNA. Due to the low solubility of rolipram in water, measurements in the presence of rolipram were carried out with 1% DMSO added to the reaction buffer. DMSO at this concentration did not interfere with enzymatic activity.

Protein Quantitation. Yields of mutant PDE2A proteins obtained by IVT were determined by Western blotting with chemiluminescent detection (Pierce Supersignal West Femto) normalized to PDE2A purified from an overexpressing strain of *E. coli* and quantitated by the Bradford method (*22*). Typically, protein obtained in an in vitro translation reaction was bound to beads. Beads were then boiled for 4 min at 93 °C with SDS-gel loading buffer containing 600 mM β-ME before loading onto a gel. Protein quantitation was done in triplicate. Total protein yields of in vitro translated wild-type PDE2A and mutants were additionally compared by band densitometry of incorporated radiolabled ^{35}S-methionine.

PCR Constructs for in Vitro Translation and Site Directed Mutagenesis. The PCR products used for IVT contained an untranslated region of at least 80 base pairs upstream of the Kozak sequence to ensure strong translation efficiency (*23*, *24*). A His_6-tag was added at the N-terminus for Ni^{2+} affinity capture of the translated proteins. PDE2A mutants were prepared using the Quik Change kit (Stratagene) with corresponding mutagenic primers Y827A 5′-AGATCGCGGAGCTGATCTACAAAGAATTCTTCTCCC-3′, Y827V 5′-AAAGATCGCGGAGCTGATCGTCAAAGAATTCTTCTCCCAG-3′, Y827F 5′-TCGCGGAGCTGATCTTCAAAGAATTCTTCTCCCA-3′, Y827M 5′-GAAAGATCGCGGAGCTGATCATGAAAGAATTCTTCTCCCAGGGA-3′, I826V 5′-GAAAGATCGCGGAGCTGGTCTACAAAGAATTCTTCT-3′, D811A 5′-GTGACCTCTCTGCCCAGACCAAGGGC-3′, Q812I 5′-AGTTGTGACCTCTCTGACCAGACCAAGGGCTGGAAGACT-3′, Q812P 5′-ACCTCTCTGACCCGACCAAGGGCTGG-3′, M847L 5′-GGCCGATGGAGCTGATGGACCGGG-3′, L858M 5′-GGCCTATATCCCTGAGATGCAAATCAGCTTCATG −5′, L858S 5′-GGCCTATATCCCTGAGTTGCAAATCAGCTTCATG-3′, L907A 5′-TTCACATCCGCGGCCTCCCAAGTAACAACTC-3′, D811A/Q812I 5′-CTAGTTGTGACCTCTCTGCCATTACCAAGGGCTGGAAGACT-3′, T819Y 5′-CCAAGGGCTGGAAGACTTACAGAAAGATCGCGGAGCTG-3′, and phPDE2ACAT plasmid as template. All mutations were verified by sequencing.

Transcription Reaction. High quality mRNA was made using the Message Machine Kit from Ambion (Austin, TX) with purified PCR products containing a T7 promoter. The mRNA was purified for further use from the inhibitory m^7G cap analogue by ethanol precipitation, resuspended in 50 μL of RNase-free water (GIBCOBRL) and loaded onto a G-50 gel filtration spin column (Amersham). mRNA concentrations were determined by UV spectroscopy. mRNA quality was found to be uniform from batch to batch, and no differences in translation efficiency could be detected.

Plasmid Construction for Bacterial Expression and Protein Purification of Human PDE2A (579−921). Human PDE2A (cGSPDE; U67733) catalytic fragment (amino acids 579−921) was cloned into pET28A using *Nhe*I and *Sal*I restriction sites to link an additional thrombin cleaving site to the N-terminus of the protein. The following primers were used: AI617F 5′-GCAGCGGCCTGGTGCCGCGCGGCAGCCATATGGCTAGC GACGATGAGTATACCAAACTTCTCCATGATG-3′, AI671R 5′-TTCCGCGGCCGCTATGGCCGACGTCGACTTATTACTCGTACTCCTCATCCAGGAAGTCCA-3′. The resulting vector pET28hPDE2A579-921 was transformed into *E. coli.* BL21(DE3). Expression of the catalytic domain was carried out in 60 mL of LB (100 mg/mL Amp) at 37 °C for 3 h after induction with IPTG (1 mM final concentration) at OD_{600} 0.7. The cells were harvested by centrifugation and resuspended in 4 mL of lysis buffer containing 50 mM Tris-HCl, 150 mM NaCl, 100 μg/mL PMSF, and 4.5 mg/mL lysozyme, pH 8.0. After 45 min incubation on ice, the cells were sonicated (VirTis, Virsonic 100) 8 times for 45 s with intervals of 1 min on ice between each sonication step. The lysate was centrifuged at 30000*g* for 10 min, and the supernatant was loaded onto a column containing 350 μL of nickel-charged Sepharose beads that had been pre-equilibrated in binding buffer (15 mM imidazole, 300 mM NaCl, 50 mM KH_2PO_4, pH 8.0). The beads were washed 3 times with 3 mL of wash-buffer (40 mM imidazole, 50 mM KH_2PO_4, 300 mM NaCl, pH 8.0) and eluted with 1 mL of elution buffer (250 mM imidazole, 50 mM KH_2PO_4, 300 mM NaCl, pH 8.0). The buffer was exchanged with storage buffer (5 mM $MgCl_2$, 100 mM Tris-HCl, pH 7.5, 2 mM β-ME, 50% glycerol) using gravity-flow Nap 10 columns (Amersham), and the protein was stored in aliquots at −80 °C. The enzymatic activity of bacterially expressed PDE2A was invariant for different batches of purified enzyme.

Plasmid Construction and Insect Cell Expression. A construct of human PDE2A was generated by PCR and subcloned into pFastBac-1 in order to generate recombinant

baculovirus using the Bac-to-Bac system (GIBCOBRL). The final protein encompasses the catalytic region starting at Ser578 and extending to Glu919. The N-terminus of the protein was modified to MetHisAla followed by the first residue Ser578 of the PDE2A sequence. The protein was expressed in SF21 insect cells infected with the recombinant baculovirus at a MOI of 0.1 and harvested 72 h after infection. Pellets of infected cells were frozen at −80 °C prior to use.

Protein Purification of Human PDE2A (578−919) from Insect Cells. Insect cell paste was resuspended (3 mL/g) in ice-cold lysis buffer (25 mM HEPES, pH 7.5; 5 mM tris-(2-carboxyethyl)phosphine hydrochloride (TCEP; Fluka); EDTA-free protease inhibitors (Roche Biochemicals; as per manufacturer's recommendations); 1 μg/mL leupeptin (Sigma); 1 mM PMSF (Roche Biochemicals); 10 μM E-64 (Roche Biochemicals)) and lysed by one passage through a chilled microfluidizer (M110L, Microfluidics International Corp., Newton, MA) at a chamber pressure of 18 kpsi. The lysate was centrifuged at 43000*g* for 30 min at 4 °C. The supernatant was concentrated 2-fold using an ultrafiltration apparatus (10K MWCO hollow fiber filter; AG Technology Corp., Needham, MA), and the buffer was subsequently exchanged by filtration with 5 volumes of lysis buffer. The filtrate was loaded onto an SP Sepharose column (Amersham Biosciences XK50/20; 50 mm i.d. × 20 cm) in tandem with a Q XL Sepharose column (Amersham Biosciences XK50/20; 50 mm i.d. × 20 cm) pre-equilibrated with lysis buffer. After loading was complete and the columns had been washed sufficiently to obtain a baseline absorbance of the eluant, the SP Sepharose was disconnected from the series and protein was eluted from the QXL resin using 20 column volumes at 1 mL/min with a 0−1 M NaCl linear gradient. Fractions containing PDE2A activity (*25*) were pooled and bound to a Blue Sepharose 6 Fast Flow column (Amersham Biosciences XK26/20; 26 mm i.d. × 20 cm) pre-equilibrated with lysis buffer. Material enriched for PDE2A was eluted with lysis buffer containing 20 mM cGMP. The material eluted from Blue Sepharose was further purified by a MonoQ HR 1010 column (Amersham Biosciences) equilibrated in lysis buffer and eluted over 20 column volumes with a 0−1 M NaCl gradient. PDE2A eluted in two peaks, which were kept separate. Peak 2 fractions were pooled on the basis of purity, as judged by SDS−PAGE analysis, and they were concentrated to 5 mL and loaded onto a Superdex HiLoad 1660 column (Amersham Biosciences) equilibrated in 25 mM HEPES, pH 7.5; 5 mM TCEP; 10 μM E64; 1 μg/mL leupeptin; and 350 mM NaCl.

Crystallization of the Catalytic Domain of Human PDE2A. Human PDE2A (residues 578−919) was purified from insect cells and crystallized by vapor diffusion. Large crystals (0.2 × 0.3 × 0.4 mm) appeared after 1−3 days when the PDE2A protein at a concentration of 10 mg/mL was mixed with an equal volume of reservoir (0.1 M Tris-HCl, pH 8.5, 0.2 M $MgCl_2$, 15% PEG 8000) at 22 °C.

X-ray Data Collection, Structure Determination, Refinement of Human PDE2A, and Metal Binding Sites. Crystals were transferred to a cryoprotectant solution made up of the reservoir solution with 15% glycerol, and then they were flash-frozen in a stream of cold nitrogen gas at 100 K. A full X-ray data set was collected from one frozen crystal at beamline X-25 of the National Synchrotron Light Source (Upton, NY). X-ray data were processed using the HKL2000 suite software (*26*). X-ray data statistics are summarized in Table 1. The structure was solved by molecular replacement methods using the program EPMR (*27*). The search model consisted of only the backbone atoms of PDE4 taken from PDB entry 1F0J (*28*), residues 152 to 461. A clear solution to the rotation and translation function searches was found using diffraction data limited to 4 Å resolution.

Table 1: Diffraction Data and Structure Refinement Statistics for the PDE2A Structure

Data Collection	
space group	$C222_1$
unit cell dimensions [*a*, *b*, *c* (Å)]	90.0, 102.5, 81.5
resolution (Å)	500.0−1.7
total number of measurements	173 939
redundancy	4
number of unique reflections	39 346
completeness (%)	97.1 (92.1)[a]
average I/σ	16.6 (2.2)[a]
R_{merge}	0.072 (0.48)[a,b]
Structure Refinement	
R factor	0.21
R_{work}/R_{free}	0.207/0.237[c]
number of reflections	37 389 (89.4%)
number of reflections used for R_{free}	3413 (8.2%)
bonds (Å)	0.004
angles (deg)	1.1
Average *B* Factor (Å^2)	
all atoms	24.1
protein (321 residues)	22.3
Zn^{2+} (1 atom)	18.9
Mg^{2+} (1 atom)	12.9
water (272 molecules)	31.4

[a] Numbers in parentheses refer to the highest resolution range (1.74−1.7Å). [b] $R_{sym} = \sum(I - \langle I\rangle)/\sum\langle I\rangle$. [c] $R = \sum||F_{obs}| - k|F_{calc}||/\sum|F_{obs}|$.

A homology model of PDE2A was then positioned according to the top rotation/translation search and subjected to refinement, followed by a combination of automatic and manual refitting. Automatic refitting was carried out using the program ArpWarp (http://www.arp-warp.org) in combination with Refmac (*29*). The refinement statistics are summarized in Table 1. The final model was refitted in the electron density with the program O (*30*) and refined with CNX (*29*) against X-ray data extending to 1.7 Å resolution (500.0−1.7 Å). The current model contains 332 out of 341 residues. Three residues at the N-terminus and 4 residues at the C-terminus of the catalytic domain are disordered and not included in the crystallographic model. Residues 900 and 901 are also disordered and hence were not built into the model. In addition, the model contains 272 water molecules and two bound metals. Based on the *B*-factor refinement, a Zn^{2+} and a Mg^{2+} ion were assigned to density peaks in the PDE2A structure. These metals are also present in PDE5. The zinc ion is coordinated by His660 (2.23 Å), His 696 (2.14 Å), Asp697 (2.16 Å), and Asp808 (2.25 Å). The Mg^{2+} ion is coordinated by Asp697 (2.30 Å) and two water molecules. The metal binding site is surrounded by helices αH6, αH7, αH8, αH10, αH11, and αH12 (Figure 2). The catalytic domain fragment of PDE2A possesses a PDE-specific motif $^{696}[HD(X)_2H(X)_4N]^{705}$ and a metal binding motif $^{656}[H(X)_3H(X)_{25}E]^{685}$ that are also present in PDE3, PDE4, and PDE5. The coordinates and structure factors for the catalytic domain of PDE2A have been deposited with the Protein Data Bank accession code 1Z1L.

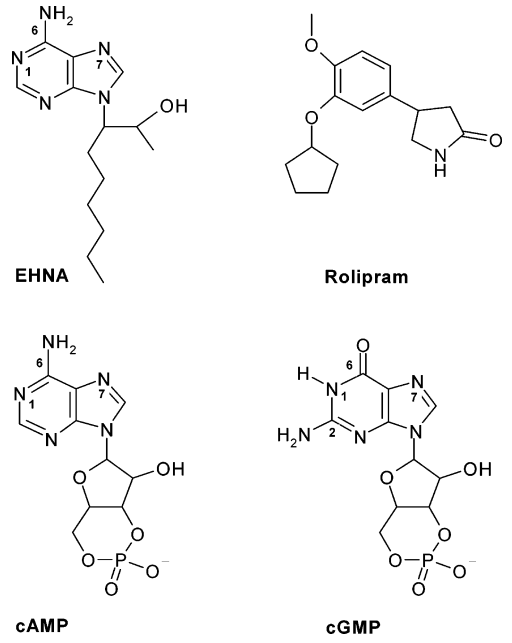

FIGURE 1: Chemical structures of inhibitors rolipram and EHNA and substrates cGMP and cAMP. Rolipram is a specific inhibitor for PDE4, and EHNA is a specific inhibitor for PDE2A. cAMP is the preferred substrate for PDE4 whereas PDE2A is substrate specific for cGMP and cAMP.

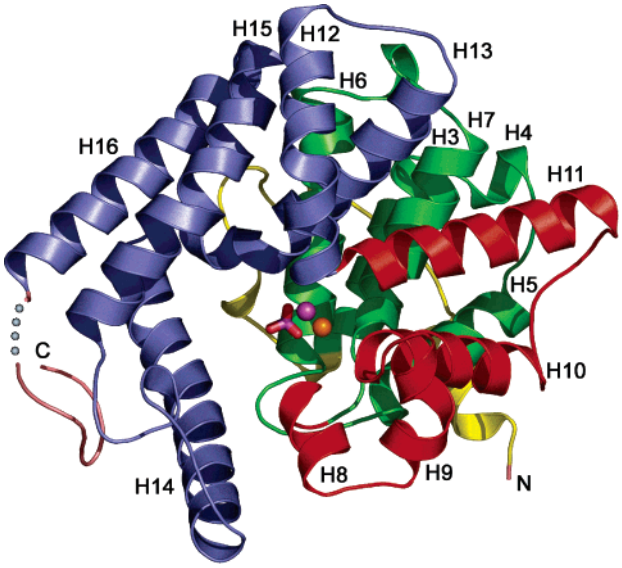

FIGURE 2: The structure of PDE2A shown as a ribbon representation. Bound Zn^{2+} and Mg^{2+} ions are shown as red and purple spheres, and the phosphate ion is shown as a stick model. Helices as well as N- and C- termini of the protein are labeled. To ease visualization, residues are shown in different colors. Residues 578−613 are represented in yellow, residues 614−700 in green, residues 701−768 in red, residues 769−898 in blue, and residues 902−915 in pink. Blue dots mark the missing amino acids at the C-terminus.

Model Generation. Models of AMP and rolipram bound in the active site of PDE2A were generated with Pymol (version 0.97) by superimposing crystal structures of PDE4 complexed with rolipram or AMP onto the crystal structure of PDE2A (*20*, *31*). Models of cGMP and EHNA in the active site of PDE2A were generated by utilizing the AMP scaffold from the crystal structure of PDE4-AMP complex as the basis for building either GMP or EHNA molecules. These models were first superimposed onto the crystal structure of unliganded PDE2A using Pymol, and then slight adjustments were made manually to relieve a few steric clashes with nearby residues of the upper binding pocket.

RESULTS AND DISCUSSION

Wheat Germ IVT System for Characterization of Partially Purified PDE2A Enzymes. The wheat germ IVT system supports the translation of a variety of prokaryotic and eukaryotic mRNAs. The system provides an alternative to bacterial expression and was used as a tool for the rapid expression of many PDE2A mutants in parallel followed by affinity capture of the translated proteins in small scale reactions. We first examined the enzymatic activity of the catalytic domain of PDE2A produced by IVT toward both cGMP and cAMP substrates and compared it to the identical protein purified from an overproducing *E. coli* strain. The yield of protein produced by the IVT systems depends on the size of the protein, the mRNA secondary structure, and solubility of the translated protein as well as parameters of the IVT system. Therefore protein yield may vary from protein to protein. For the catalytic domain constructs of PDE2A the yield is ∼280 ng per 100 μL reaction in 25 min, and this is consistent for all experiments. Bacterial cultures produced ∼2−3 μg of protein per 100 μL culture volume (data not shown, for growth conditions see Experimental Procedures). PDE2A protein expressed from insect cells was obtained with yields of ∼5 mg/L, and protein from insect cells was 5−10 times more active than bacterially expressed protein (data not shown, for growth conditions see Experimental Procedures). The proteins obtained from bacterial or IVT expression showed similar K_m values for cGMP (34 μM_{bac} and 43 μM_{IVT}) and cAMP (32 μM_{bac} and 34 μM_{IVT}). These values for the catalytic domain are in the range of published literature values for full length PDE2A (cAMP 30−50 μM, cGMP 10−50 μM) (*32*, *33*). The bacterially expressed catalytic domain of PDE2A exhibits a 14-fold higher k_{cat} value for cGMP than for cAMP and a 12-fold higher k_{cat}/K_m value for cGMP than for cAMP (Table 2). In vitro translated protein showed a 5-fold higher k_{cat} value for cGMP in comparison to cAMP and a 4-fold higher affinity for cGMP. The slight differences in k_{cat} values of PDE2A produced by IVT and bacterial expression might be caused by the different purification procedures and/or differences in the fraction of active molecules.

No background phosphodiesterase activity was detected in association with Ni-NTA beads incubated with a mock IVT reaction or with inactive mutants of PDE2A affinity purified from wheat germ extracts. The enzymatic activity of immobilized PDE2A was constant for at least 45 min under these assay conditions at RT. The affinity purified proteins could be stored for at least 2.5 h in reaction buffer at 4 °C without a significant loss of enzymatic activity (data not shown). These results were highly reproducible, with different batches of wheat germ extract producing similar amounts of protein with comparable activities.

The IVT system was shown to be a convenient and powerful tool for the initial survey of enzymatic activities. By combining IVT expression with a rapid activity assay, the enzymatic properties of a large number of PDE2A mutants could be quickly surveyed. This approach made use of PCR-generated templates and affinity capture of the translated products and thus avoided the time-consuming

Table 2: Kinetic Parameters of Wild-Type hPDE2A Catalytic Domain (579−921)[a]

	K_m, μM		k_{cat}, s^{-1}		k_{cat}/K_m, s^{-1} M^{-1}(10^{-3})	
protein	cGMP	cAMP	cGMP	cAMP	cGMP	cAMP
in vitro translated	43 ± 7	34 ± 6	0.6 ± 0.1	0.12 ± 0.01	14 ± 3	3.4 ± 0.7
bacterially expressed	34 ± 4	32 ± 8	4.2 ± 1.5	0.3 ± 0.1	124 ± 40	9.4 ± 3.3

[a] Apparent K_m values were determined from direct plots of v_0 versus [S]. The results represent the average of at least two independent determinations measured in triplicate ± standard deviation.

process of traditional cell based protein production and purification. Wheat germ extract can be inexpensively produced in large quantities, enabling large format experiments to be pursued economically. The components of the IVT reaction can be individually optimized for maximum translation efficiency of a particular protein. We used this approach to explore the specificity determinants of PDE2A, using a crystal structure of the catalytic domain of PDE2A as a guide to mutagenesis.

Crystal Structure of the Human PDE2A Catalytic Domain and Its Comparison with PDE3, PDE4, and PDE5 Structures. The structure of the PDE2A catalytic domain (amino acids 578−919) was determined and refined to 1.7 Å resolution in the space group $C222_1$ (R_{work} 21% and R_{free} 24%, Table 1). The structure contains one protein molecule per asymmetric unit, and the crystal packing arrangement gives no indication of a physiologically relevant dimer. This is consistent with the proposal that PDE2A dimerization is mediated by the first GAF domain (*11*), which is not present in the fragment that was crystallized. The catalytic domain is composed of fifteen α-helices and six 3_{10} helices arranged in a compact fold. The nomenclature for helices in the crystal structure of PDE4D was adopted for the PDE2A structure (Figure 2) (*20*). Three subdomains are evident in the protein fold of the catalytic domain. Residues 614−700 (H3−H7, colored in green in Figure 2 and Figure 3) form the first subdomain, residues 701−768 (H8−H11, colored in red in Figure 2 and Figure 3) form the second subdomain, and residues 769−899 (H12−H16, colored in blue in Figure 2 and Figure 3) form the third subdomain. No electron density was observed for residues 900 and 901, which apparently comprise a flexible loop between helix 16 and the C-terminal residues (902−915) colored in pink in Figure 2 and Figure 3. More than 230 equivalent Cα atoms from PDE2A could be superimposed on structures of PDE4 (RMSD 1.4 Å), PDE3 (RMSD 1.2 Å), and PDE5 (RMSD 0.98 Å). The overall structure of PDE2A is very similar to that of PDE3B, PDE4D, and PDE5A. The sequence identities between PDE2A and PDE3B, PDE4D, and PDE5A are 21.3%, 25.1%, and 32.8%, respectively (Figures 4 and 5). However, the PDE3 and PDE4 structures show localized differences from PDE2A, mainly in the positions of helices H0 and H3. It is possible that the N-terminal truncation and absence of a GAF domain in the proteins that were crystallized may compromise packing interactions, causing these helices to become slightly dislocated. Additionally, PDE3 contains an insert of 44 residues between helices H6 and H7 and a 52 residue insert between helices H15 and H16 that are not present in PDE2A (Figure 4). Given the overall conservation of the PDE structures across the PDE gene family and the absence of a PDE2/inhibitor complex structure, we used liganded structures of other PDEs to identify potential specificity determinants in PDE2A.

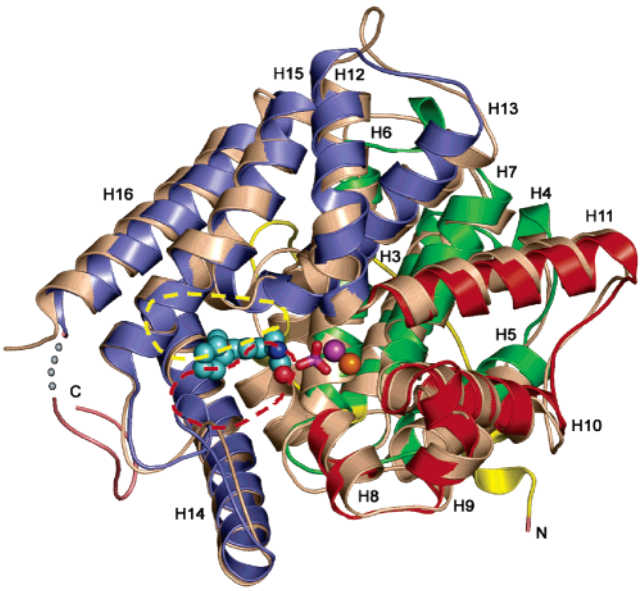

FIGURE 3: Structure alignment of PDE2A with PDE4D. The PDE4D structure is in complex with rolipram (*31*). A total of about 234 equivalent Ca atoms are superimposed between PDE2A and PDE4 structures with a RMS distance of 1.4 Å. The PDE2A structure is shown in the same orientation as in Figure 1 and colored the same way. The PDE4D structure is colored salmon, and inhibitor rolipram bound to PDE4D is drawn as a turquoise space filling model. Mg^{2+} and Zn^{2+} are shown as violet and orange spheres, respectively. Blue dots mark the missing amino acids at the C-terminus. Red dashed lines indicate the location of the lower binding pocket residues, yellow dashed lines the location of the upper binding pocket residues in PDE2A.

The active site structure of PDE2A was compared with the structure of PDE4D in complex with rolipram (*20*) (Figure 3). The active site lies mainly within the third subdomain and is bounded by helices H15 and H14, the C-terminus of H13, a 3_{10} helix between helices H13 and H14, the C-terminus of H5, the N-terminus of H6, and the loop region between H5 and H6. The residues that line the substrate binding pocket of PDE2A are Tyr655, His656, Leu809, Asp811, Gln812, Thr819, Ala823, Ile826, Tyr827, Phe830, Met847, Leu858, Gln859, Phe862, Ile866, and Leu907 (Figure 4). The binding pocket itself can be divided into an upper and lower binding pocket. The upper binding pocket consists of residues Leu809, Asp811, Gln812, Thr819, Gln859, Phe862, and Ile866. The lower binding pocket consists of residues Ala823, Tyr655, Ile826, Tyr827, Phe830, Met847, Leu858, and Leu907.

Recently, the structures of PDE1, PDE3, PDE4, PDE5, and PDE9 with products in the active site have been published, and many determinants of substrate specificity have been identified for these PDEs (*34*−*38*). A key residue for substrate binding in the PDE family was identified as a conserved glutamine residue. The equivalent residue in PDE2 is Gln859, which has the potential to form a hydrogen bond

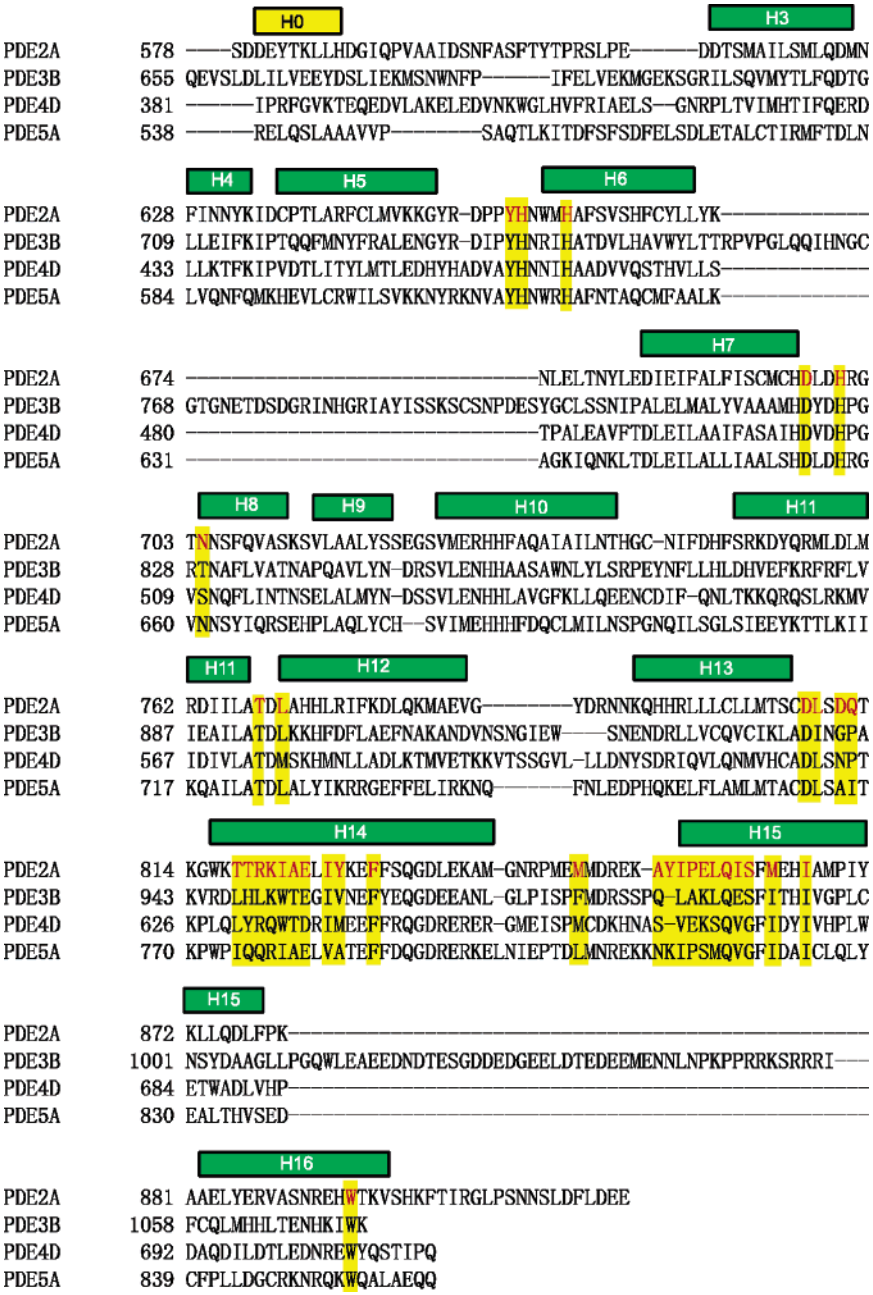

FIGURE 4: Structure based sequence alignment of PDE2A, PDE3B, PDE4D, and PDE5. The PDE4D structure is in complex with rolipram (*31*). Superposition of this structure with PDE2A revealed residues in PDE2A that are in close proximity to rolipram. These residues define the binding pocket of PDE2A and are colored red.

with the exocyclic amino group (NE2) of cAMP or the exocyclic carbonyl oxygen (OE1) of cGMP by switching the orientation of the side chain. In PDE4, the conserved glutamine forms a hydrogen bond with Tyr329 and stabilizes the tyrosine in a conformation appropriate for cAMP binding. The substrate specificity of PDE5 for cGMP is determined by a hydrogen bond between the conserved glutamine and residue Gln775 (*34*). Thus, the different substrate specificities of PDE4 and PDE5 can be explained in part by different interactions of the conserved glutamine with nearby residues of both enzymes. The dual substrate specificity of PDE1B is determined by a hydrogen bond network between the neighboring residue His381 and residues His373 and Trp496. None of these residues forms a hydrogen bond with the conserved Gln421 (*34*). The equivalent residue to His381 in PDE2A is Thr819. Thr819 might interact with the conserved Trp895 through van der Waals interactions and a possible hydrogen bond between the nitrogen of the tryptophan and the hydroxyl group of threonine (distance of 3.7 Å after side chain rotation). Thr819 is too far from the conserved residue Gln859 for a hydrogen bonding interaction (distance of 4.5 Å). The side chain of Gln859 is therefore free to rotate, and could exchange the positions of the (OE1) carbonyl oxygen and (NE2) amino group to accommodate either cGMP or cAMP (Figure 6A). Additionally, Gln859 may form two hydrogen bonds to the N1 and O6 atoms of purine cyclic nucleotides and could therefore stabilize either substrate in the binding pocket. As in other PDEs, the substrate specificity of PDE2A may also depend on an additional network of residues in the close neighborhood of the glutamine residue. Noteworthy is Tyr827, located in the lower binding pocket of PDE2A, which is in hydrogen

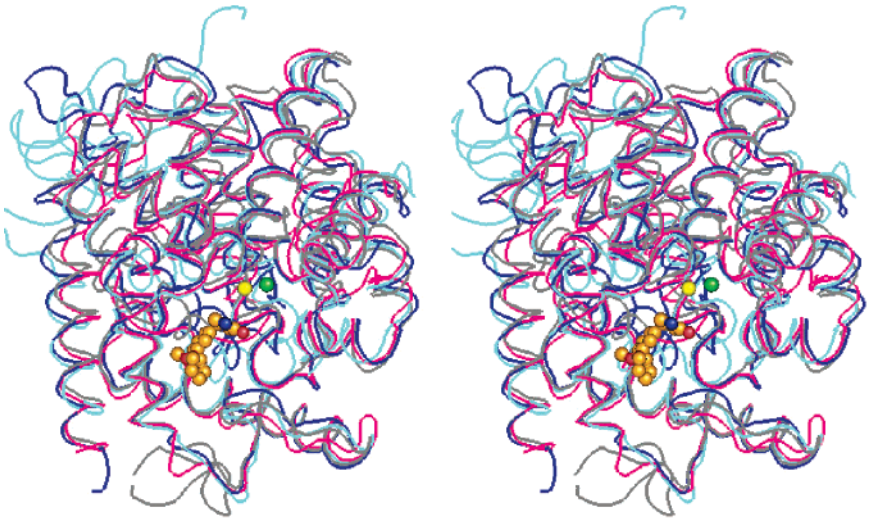

FIGURE 5: Stereoview of the superposition of PDE2A (brown ribbon), PDE3B (turquoise ribbon), PDE4D (blue ribbon), and PDE5A (red ribbon) with rolipram (ball-and-stick) bound in the catalytic domain of PDE4. The metal ions are represented as green and yellow spheres.

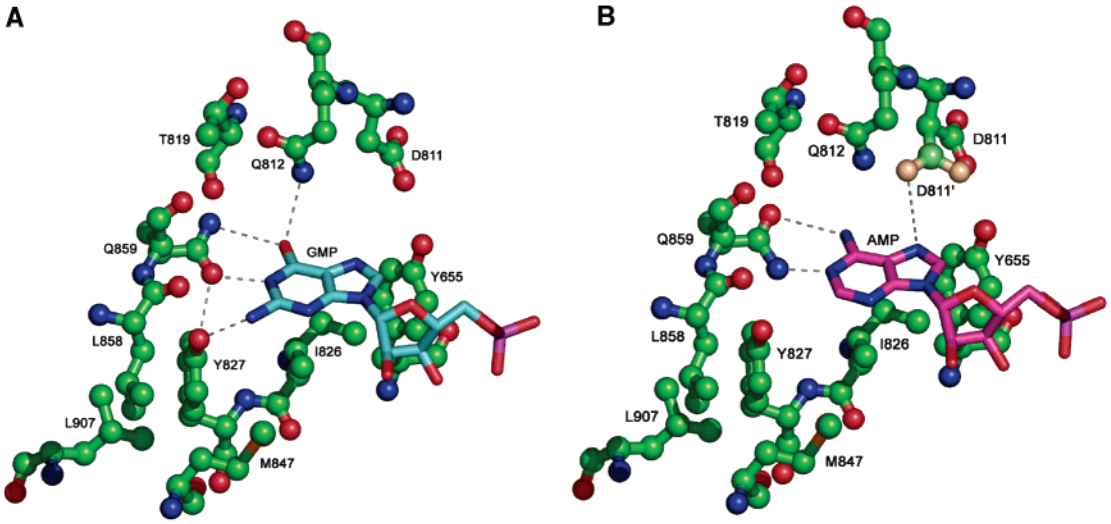

FIGURE 6: Models of GMP and AMP docked into the crystal structure of PDE2A. (A) In the crystal structure of unliganded PDE2A, the side chain of Gln859 adopts an orientation that is compatible with binding to GMP. We have modeled the complex with GMP by superimposing PDE2A onto the crystal structure of PDE4-AMP and modifying the AMP scaffold to GMP. In this orientation, the (OE1) carbonyl oxygen of Gln859 can accept a hydrogen bond from the N1 atom of guanidine, whereas the (NE2) amino group of Gln859 can donate a hydrogen bond to the O6 exocyclic carbonyl oxygen of the guanidine ring. The exocyclic amino group of the guanidine ring donates another hydrogen bond to the (OE1) oxygen of Tyr827. The hydroxyl group of Tyr827 donates a hydrogen bond to the (OE1) carbonyl oxygen of Gln859. We propose that Gln812 supports cGMP binding by donating a hydrogen bond to the O6 exocyclic carbonyl oxygen of the guanidine ring. (B) The side chain of Gln859 could flip to accommodate cAMP. In this modeled conformation, the Gln859 side chain donates a hydrogen bond to the N1 adenine nitrogen and accepts a hydrogen bond from the exocyclic N6 of adenine. Furthermore, an alternative conformation of the Asp811 side chain termed Asp811′ would enable a hydrogen bond to be donated to N7 of adenine.

bonding distance to Gln859 (distance of 3.1 Å) and may form a hydrogen bond with the (OE1) carbonyl oxygen of Gln859.

Selection of Active Site Residues for Mutation Analysis. An inspection of all superimposed residues of PDE2A and PDE4 that are in close contact with rolipram reveals a small structural difference in the upper binding pocket of PDE2A (Figure 7A). The upper binding pocket of PDE2A is less sterically restricted than PDE4, whereas the lower binding pocket appears to be more encumbered. To analyze the involvement of residues from these two active site pockets in catalysis and inhibition, a total of eight residues were selected for mutagenesis experiments. Three residues, Asp811, Gln812, and Thr819, from the upper binding pocket and five residues, Ile826, Tyr827, Met847, Leu858, and Leu907, from the lower binding pocket were chosen for mutagenesis (Table 3A). Using the aligned sequences of PDEs from different functional families, specific amino acid substitutions were selected either to introduce a drastic change within the binding pocket or to mimic amino acid environments of other PDEs in PDE2A.

Effects of Mutagenesis on PDE2A Activity. The wheat germ IVT system was used to express the selected mutants and compare their activities with that of wild-type PDE2A (Table 3B). Most of the mutants showed decreased activity toward both cAMP and cGMP. Some mutants were inactive toward cGMP, such as Leu907Ala, Met847Leu Tyr827Met, Tyr827Ala, Gln812Pro, and Thr819Tyr. Others showed no activity toward cAMP, such as Leu858Ser, Tyr827Met, Tyr827Ala, Tyr827Val, Tyr827Phe/Leu907Ala, Thr819Tyr, Gln812Pro, and Gln812Pro/Thr819Tyr. Presumably, these

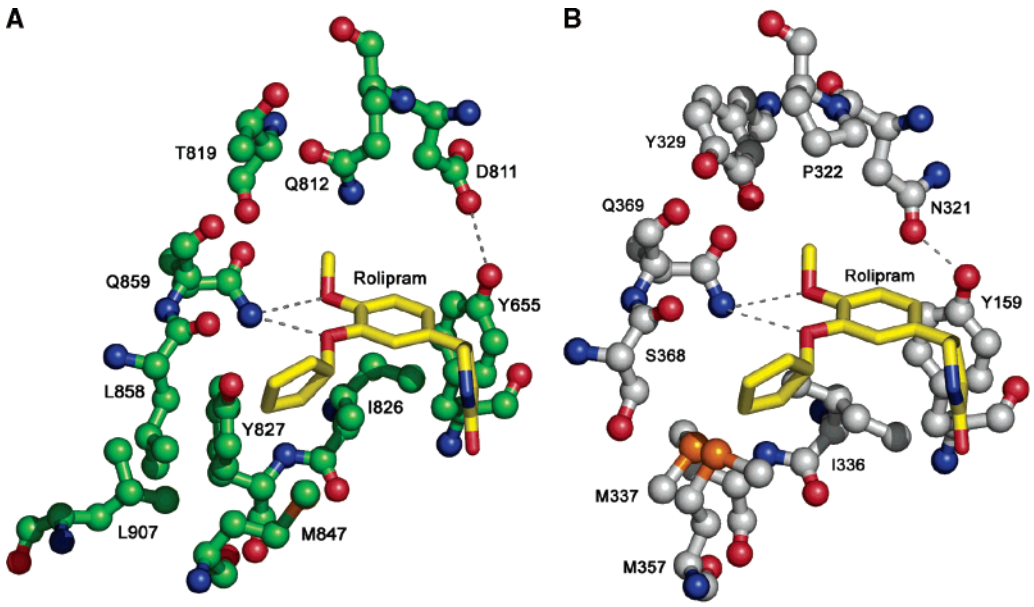

FIGURE 7: (A) Rolipram interactions with active site residues of PDE2A. Rolipram is docked into the crystal structure of PDE2A by superimposing the crystal structure of PDE4 complexed with rolipram on the crystal structure of PDE2A. A hypothetical hydrogen bond to Tyr655 is represented as a dashed line. No equivalent residue is available for L907 in PDE4D. (B) Active site residues of crystal structure of PDE4D in close proximity to rolipram.

mutations have disturbed the active site and interfere with substrate binding or the positions of catalytic groups. Only the Ile826Val mutant protein showed increased activity toward cGMP (Table 3B). However, all of these mutants were expressed as soluble proteins, with yields similar to that of the wild-type protein as determined by Western blot analysis. Due to the very low activity toward cAMP, we decided to use cGMP as a substrate for analyzing the inhibition profiles of the mutants. The K_m values for the least and most active mutants were measured for substrates cAMP and cGMP, and there was no significant deviation (±20%) compared to the K_m value of wild-type protein. Therefore, all mutants were measured at the same subsaturating concentration of cGMP.

Effects of Mutagenesis on Substrate Specificity. The substrate specificities of different PDEs are thought to be correlated with the position of a conserved glutamine residue in the upper binding pocket (*34*). However, dual substrate specificity is thought to result from a network of interactions involving residues around the glutamine that influence catalytic activity.

An initial screen for activity toward cGMP and cAMP revealed that the mutations Gln812Ile, Asp811Ala, and [Asp811Ala/Gln812Ile] strongly influenced substrate specificity. These mutants all retained more than 50% activity compared to wild-type PDE2A (Table 3B). The substituted residues are all located in the upper binding pocket, in close proximity to the conserved residue Gln859 that strongly influences substrate binding specificity. The activity data for PDE2A mutants toward substrates cGMP and cAMP indicates that Gln812 selectively affects cGMP conversion (Table 3B). The Gln812Ile mutant showed a lower activity toward cGMP, whereas its activity toward cAMP was unaffected. We think that the upper binding pocket residues of PDE2A may rotate their side chains upon binding for either of the substrates cAMP and cGMP. One of these side chain rotations might be energetically more favorable for one of the substrates. Hence, the mutation of Gln812Ile could bias the orientations of upper binding pocket residues to favor binding of cAMP in preference to cGMP. Therefore we could see a reduced activity for cGMP and no decrease in activity for cAMP.

Superposition of the crystal structure of PDE4D complexed with product AMP on PDE2A suggested that cAMP may have slightly different binding interactions in the substrate pocket of PDE2A (Figure 6B). The adenine ring of cAMP could form two hydrogen bonds with Gln859 by rotating the Gln859 side chain relative to its orientation in the unliganded crystal structure. The model shows that Gln812 might be unable to interact with the exocyclic N6 amino group of the adenine ring, providing an explanation for the unchanged activity of the mutant Gln812Ile toward cAMP (Table 3B).

On the other hand, mutant Asp811Ala shows a reduced activity for cAMP, but its activity for cGMP is unaffected. In the apo structure of PDE2A Asp811 forms hydrogen bonds with Arg608 and Tyr655 (distance of 3.3 and 3.1 Å). Our modeling suggests that Asp811 could make a hydrogen bond with cGMP and cAMP if its side chain were allowed to rotate. The apo structure of PDE4 shows two hydrogen bond interactions of Asn321 (Asp811 in PDE2A) with Tyr159 and Asp167. A comparison with the crystal structure of PDE4 with AMP bound in its active site and the PDE4 apo structure shows that the side chain of Asn321 has rotated toward the adenine ring upon AMP binding to form hydrogen bonds with the exocyclic amino group and the N7 nitrogen (*28*, *31*, *39*). Once a substrate enters the active site of PDE2A, Asp811 may forsake the hydrogen bond interaction with the positively charged arginine and instead rotate toward the purine ring to interact with the N7 nitrogen, stabilizing the interaction of the purine ring with the upper binding pocket. This is indicated with the alternative side chain conformation Asp811′ of Asp811 in Figure 6B. This would be in accordance with the decreased activities of mutant Asp811Ala toward substrate cAMP (Table 3B). The double mutation [Asp811Ala/Gln812Ile] should interrupt hydrogen bond

Table 3: Sequence Alignment of the Human PDE Family and Mutations in the Active Site of PDE2A and Their Activity Comparison

(A) Sequence Alignment of the Human PDE Family[a]

protein	811	812	819	826	827	847	858	907
PDE2A	D	Q	T	I	Y	M	L	L
PDE1A	H	P	H	L	M	L	S	M
PDE3A	G	P	H	I	V	F	L	G
PDE4D	N	P	Y	I	M	M	S	L
PDE5A	A	I	Q	V	A	L	M	I
PDE6A	A	I	Q	V	A	M	L	K
PDE7A	N	P	S	V	T	L	I	D
PDE8A	N	P	C	I	S	V	S	R
PDE9A	N	E	A	L	L	F	A	E
PDE10A	S	V	T	I	Y	M	G	W
PDE11A	A	V	Y	V	T	I	L	L

(B) Mutations in the Active Site of PDE2A and Their Activity Comparison

mutant	811	812	819	826	827	847	858	907	cGMP[c] activity	cAMP[c] activity
PDE2A WT	D	Q	T	I	Y	M	L	L		
D811A	A								=	↓
D811A/Q812I[b]	A	I							↓	↓
Q812I		I							↓	=
Q812P		P							↓↓	↓↓
Q812P/T819Y[b]		P	Y						↓↓	↓↓
T819Y			Y						↓↓	↓↓
I826V				V					↑	↓
Y827A					A				↓↓	↓↓
Y827V					V				↓↓	↓↓
Y827M					M				↓↓	↓↓
Y827F					F				↓	↓↓
Y827F/L907A[b]					F			A	↓↓	↓↓
M847L						L			↓↓	↓↓
L858M							M		↓	↓↓
L858S							S		↓↓	↓↓
L907A								A	↓↓	↓↓

[a] Residues selected for mutation studies are shown. [b] Double mutations. [c] Mutant activity compared to wild-type based on equal amounts of translated protein under saturating substrate conditions; = activity similar to wild-type; ↑ activity higher than wild-type; ↓ activity higher than 50%; ↓↓ activity less than 20%; ↓↓↓ activity less than 10% or mutant inactive. Activities were determined in triplicate in two independent experiments.

interactions with cGMP as well as with substrate cAMP. This prediction is borne out by the lower enzymatic activities of the double mutant [Asp811Ala/Gln812Ile] toward both cGMP and cAMP (Table 3B). Although the loss of a hydrogen bond might impact substrate binding affinity, nearby hydrophobic residues may also contribute interactions with the bound substrates and the loss of a hydrogen bond might be compensated by a more hydrophobic environment in the mutant enzyme.

We also focused on mutations of residue Tyr827 located in the lower binding pocket of PDE2A. Tyr827 is the only nearby residue that is capable of forming a hydrogen bond with the conserved residue Gln859 (distance of 3.1 Å). Our docking model of GMP in the active site of PDE2A predicts another hydrogen bonding interaction of the hydroxyl group of Tyr827 with the exocyclic 2-amino group of GMP in addition to hydrogen bond interactions contributed by Gln812 and Gln859 in the upper binding pocket (Figure 6A).

We further investigated the influence of Tyr827 on the activity toward cGMP by mutating this residue to alanine, valine, or methionine. These mutations eliminated activity toward cGMP. However, the conservative Tyr827Phe mutation was compatible with low activity toward cGMP, although no activity was observed with cAMP. The activity toward one of the substrates might be influenced by the rearrangement of the neighboring residues of Gln859. Tyr827 may form hydrogen bonds with either the amino group or the carbonyl oxygen of the Gln859 side chain. The side chain of the neighboring residue Thr819 does not interact with Gln859 in the apo structure. However, Thr819 might interact with Trp895 via van der Waals interactions. The loss of an interaction with a tyrosine hydroxyl in the Tyr827Phe mutant could allow Gln859 to shift toward the upper binding pocket and interact with Thr819, while preserving the interactions of Gln859 with cGMP. In the Tyr827Phe mutant, the proposed interaction of Gln859 with Thr819 could partially compensate for the lost interaction with Tyr827, and it may impair the rotation of Gln859 to accommodate cAMP, explaining the loss of detectable activity toward this substrate (Table 3B). This mutation might also change the orientations of residues in the lower binding pocket near the purine ring of the substrate.

On the basis of the structure of PDE2A and our model for GMP complexed in the active site, it appears that Tyr827 may play two important roles: it participates in a hydrogen bonding network with the purine ring of cGMP, and it sterically impinges on the lower binding pocket. A comparison of the aligned sequences of all PDEs showed that only two enzymes, PDE2 and PDE10, contain a tyrosine at this position (Table 3A). PDE10 similarly exhibits dual substrate specificity for cGMP and cAMP, with a 27-fold lower K_m for cAMP vs cGMP and a 2-fold higher V_{max} for cGMP (*40*, *41*). The higher enzymatic rates of PDE2A and PDE10 toward cGMP relative to cAMP might be explained by stabilizing contacts of the tyrosine that position cGMP for interaction with Gln812. However, Tyr827 apparently does not contribute to binding of the cAMP substrate.

Residue Ile826 is located in close proximity to Tyr827 in the lower binding pocket of PDE2A. Mutation of Ile826 to valine increased the activity toward cGMP and decreased the activity toward cAMP compared to the wild-type enzyme (Table 3B). We assume that residue Ile826 influences substrate selectivity indirectly, by positioning the substrate within hydrogen bonding distance of residues in the upper binding pocket, particularly Gln859. A smaller residue at position 826 may fail to stabilize substrate binding for optimal interactions with the upper binding pocket. This would be in accordance with the observed decrease in cAMP activity and increased cGMP activity of the Ile826Val mutant (Table 3B).

Effects of Mutagenesis on Inhibitor Specificity and Selectivity. We next explored how specific residues in the active site of PDE2A influence binding to the inhibitors EHNA and rolipram. EHNA is a commercially available inhibitor that is specific for PDE2, with an IC_{50} value of 1 μM (*3*). The core structure of EHNA resembles cAMP, a substrate for PDE2. EHNA differs from cAMP, with a bulky hydrophobic carbon side chain replacing the ribose moiety (Figure 1). The inhibitor rolipram is specific for PDE4, and its overall structure is strikingly different from that of EHNA. Rolipram consists of a pyrrolidone group, a cyclopentyloxy group, and a phenyloxy group, which all contribute to the hydrophobicity of this compound (Figure 1). We chose rolipram over other available inhibitors because of the structural similarity of PDE2A with PDE4D, which makes the crystal structure of

Table 4: Potency of Selected PDE Inhibitors against hPDE2A Wild-Type and Mutant Proteins[a]

protein	IC_{50}, μM	
	EHNA	rolipram
wild-type	0.61 ± 0.15	150 ± 23
D811A	3.64 ± 0.52	80 ± 47
D811A/Q812I	0.72 ± 0.31	30 ± 6
Q812I	0.89 ± 0.17	79 ± 29
I826V	3.2 ± 1.1	250 ± 55
Y827F	1.5 ± 0.5	197 ± 51
L858M	0.8 ± 0.1	90 ± 18

[a] IC_{50} values were determined at a cGMP concentration of 3 μM and 9 different inhibitor concentrations. The results represent the average of at least two determinations (measured in triplicate) ± standard deviation from at least two independent wheat germ preparations.

PDE4D complexed to rolipram a valuable guide to studies of PDE2A. Additionally, the interactions of PDE4 family members with rolipram and cAMP are well characterized by mutation and crystal structure analyses (*20*, *42*, *43*).

Inhibition by Rolipram. As expected, wild-type PDE2A is insensitive to rolipram, with an IC_{50} value of 150 μM. However, the double mutation Asp811Ala/Gln812Ile in the upper binding pocket caused a statistically significant 5-fold reduction in the IC_{50} value for rolipram (Table 4). Single mutations of both residues caused only a 2-fold decrease in IC_{50} for rolipram. Replacement of Gln812 with isoleucine increases the hydrophobicity of the upper binding pocket without changing the steric constraints on substrate and inhibitor binding. However, this hydrophobic residue substitution might improve rolipram binding and explain the lowered IC_{50} value. This conclusion is also in accordance with the potent inhibition of PDE4 by rolipram, which has a proline at the equivalent position of Gln812 in PDE2A (Figure 7B) and is part of the hydrophobic clamp pocket formed by Phe372 and Ile336 in PDE4 (*44*). We predicted that introduction of a proline at position 812 would mimic the binding pocket of PDE4 and similarly decrease the IC_{50} for rolipram. However, the proline substitution for Gln812 in PDE2A resulted in loss of detectable activity toward both cGMP and cAMP (Table 3B). One possible explanation is that the Gln812Pro mutation opened up the binding pocket of PDE2A even more, compromising the binding affinity of the substrate.

Interestingly, PDE5 is not significantly inhibited by rolipram, and it possesses hydrophobic residues Ala767 and Ile768 as corresponding residues to Asp811 and Gln812 in PDE2A. However, the environment of PDE5 contains other residues that might influence inhibitor binding. Residues that differ from PDE2A are Gln775, Val782, and Ala783 (Thr819, Val826, and Tyr827 in PDE2A). These residues would be in close contact to rolipram. Gln775 forms hydrogen bonds with the conserved residue Gln817 and residue Trp853 determining substrate specificity for PDE5 (*34*). Therefore, it might not take part in inhibitor binding. Although residues Ala767 and Ile768 create a more hydrophobic environment for rolipram in PDE5, these two residues alone are obviously not sufficient for rolipram binding. Tyr827 in PDE2A may strongly influence rolipram binding, by sterically hindering rolipram from accessing the active site. The equivalent residue in PDE5 is an alanine (Ala783), which may be too small to shape the lower binding pocket for van der Waals interactions with rolipram. Additionally, residue Val782 in PDE5 might influence the position of rolipram more strongly than residue Ile826 of PDE2A or the valine substituted in Ile826Val. Interestingly, the equivalent residue to Val782 is Ile336 in PDE4 and is part of a hydrophobic clamp pocket for pyrazole derivatives (*44*). However, the binding pocket of PDE5 might be too large to interact favorably with rolipram because Val782 and Ala783 are smaller than their counterparts in PDE4 and PDE2. This structural difference in the lower binding pocket could explain why rolipram does not inhibit PDE5.

The mutation of Asp811 to alanine may have an additional influence on rolipram binding in the active site (Table 4). In our model, the phenyl group of rolipram occupies the neighborhood of Asp811. A change of Asp811 to alanine would introduce an additional hydrophobic environment for rolipram in the binding pocket formed by residues Leu809, Ile866, Phe862, and Thr818. Furthermore, the Asp811Ala mutation may interrupt a hydrogen bond between Asp811 and Tyr655. Residue Tyr655 is located adjacent to the pyrrolidone group of rolipram in the modeled complex (Figure 7A). Loss of the hydrogen bond with Asp811 could release Tyr655 and make more space for the pyrrolidone group of rolipram. The proposed movement of the Tyr655 side chain could also decrease steric interference in the lower binding pocket of the active site. In our model of rolipram docked into the crystal structure of PDE2A (Figure 7A), Tyr827 is in close proximity to the cyclopentyloxy group of rolipram and might interfere with the inhibitor binding. A methionine occupies this position in PDE4, where it encroaches on the lower binding pocket (Figure 7B).

To investigate the influence of Tyr827 on inhibitor binding, this residue was mutated to alanine, valine, and phenylalanine. Only the conservative substitution Tyr827Phe retained detectable enzymatic activity, but this did not affect rolipram binding (Figures 3B and 4). In fact, the IC_{50} value for Tyr827Phe is similar to that of wild-type PDE2A. In an effort to create the same amino acid environment that exists in PDE4, Tyr827 was also mutated to methionine. However, this mutation caused a complete loss of activity toward cGMP (Table 3B). This finding suggests that Tyr827 sterically interferes with rolipram binding to PDE2A by limiting space for the cyclopentyloxy group. The double mutation [Asp811Ala/Gln812Ile] may enhance rolipram binding not only by increasing hydrophobicity of the pocket but also by removing the steric interference of Tyr827 with rolipram.

Inhibition by EHNA. We also analyzed the effects of active site mutations on the inhibitory potency of EHNA. Wild-type PDE2A expressed by IVT was inhibited by EHNA (IC_{50} = 0.61 μM), in accord with previously reported values (*3*). The mutations Asp811Ala and Ile826Val were the only amino acid substitutions that significantly affected inhibition by EHNA (Table 4). The mutation of Asp811 to alanine increased the IC_{50} value for EHNA 6-fold. The Ile826Val mutant was inhibited by EHNA with 5-fold lower potency than wild-type PDE2A (Table 4). Since the structure of EHNA bears resemblance to AMP, a comparison of PDE2A with the crystal structure of AMP bound to PDE4D may suggest how these residues affect the IC_{50} values.

The crystal structure of AMP complexed with PDE4D shows a conformational change, and four interactions (with

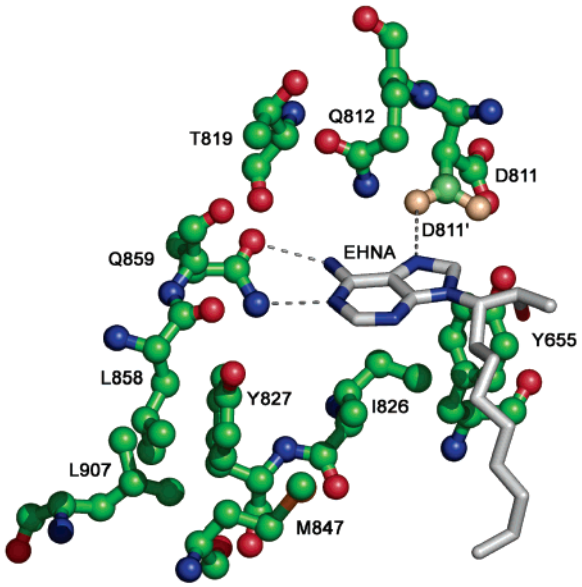

FIGURE 8: Docking model of EHNA with PDE2A residues. Hydrogen bonds are shown in black for EHNA interactions with conserved PDE2A residue Gln859 and an interaction between an alternative modeled conformation of Asp811, Asp811′, and the N7 nitrogen of adenine.

N1, N7, and the exocyclic N6 positions) of the adenine ring of AMP contributed by Gln369 and Asn321 (*31*, *34*, *39*). In fact, our docking model of EHNA in the active site of PDE2A shows that EHNA may interact with the analogous active site residues of PDE2A, Gln859, and Asp811′ (the modeled conformation of the Asp811 side chain), to form hydrogen bonds (Figure 8). EHNA is in close proximity to Gln859, which could donate two hydrogen bonds to the N1 and N6 nitrogens of the adenine ring. On the other side of the binding pocket, Asp811 (equivalent to Asn321 in PDE4) could donate another hydrogen bond to N7 of the adenine ring in order to stabilize the bound inhibitor. This hypothesis is supported by the observation that the Asp811Ala mutant has decreased activity toward cAMP, whereas activity toward cGMP was unchanged (Table 3B). Interestingly, the additional mutation of Gln812Ile restores the inhibitory potency of EHNA in the [Asp811Ala/Gln812Ile] double mutant (Table 4). One explanation for this is that the hydrophobic residue substitutes in the upper binding pocket of the double mutant provide favorable van der Waals interactions with EHNA. Although hydrogen bond interactions with Asp811 might be eliminated by alanine, the more hydrophobic environment counterbalances this effect.

Asp811 may also form a hydrogen bond with Tyr655 (distance of 3.3 Å). The Asp811Ala mutation would eliminate a hydrogen bond with Tyr655, freeing the tyrosine hydroxyl group to accept another hydrogen bond from the hydroxyl group of EHNA. The loss of the interaction between Asp811 and Tyr655 could allow the side chain of Tyr655 to rotate away from the purine ring of EHNA. The hydrogen bonding distance would therefore increase and EHNA binding might be destabilized, resulting in a higher IC_{50} value.

Our results indicate that Asp811 plays an important role in EHNA selectivity for PDE2A (Table 4). A comparison to PDE10 could elucidate the basis of this effect. PDE10 possesses 42% sequence similarity to PDE2A and 47% similarity to PDE5 within the catalytic domain. PDE10 is specifically inhibited by dipyridamole, with an IC_{50} value of 1.2 μM (*41*). Ser667 of PDE10 is equivalent to Asp811 in PDE2A, one of four residues (Asp811, Gln812, Gly858, and Trp907) that are different in the catalytic domains of PDE2A and PDE10 (Table 3A). Two of these four residues are in the upper binding pocket (Asp811, Gln812), and two are in the lower binding pocket (Gly858, Trp907). The residues in the lower binding pocket may lie too far away for interaction with the inhibitor and therefore might be irrelevant for EHNA selectivity. Despite the very similar amino acid sequences of PDE2A and PDE10, EHNA does not inhibit PDE10 ($IC_{50} > 100$ μM) (*40*). Therefore, one or both residues in the upper binding pocket that differ in PDE10 should have an influence on the inhibitor specificity for EHNA. In contrast to PDE2A, we assume that Tyr514 of PDE10 (equivalent to Tyr655 of PDE2A) does not accept a hydrogen bond from Ser667. Hence, if rotation of the Tyr514 side chain is unencumbered, this side chain could sterically interfere with EHNA binding.

The other distinguishing residue in the upper binding pocket of PDE2A is Gln812, which is analogous to Val668 in PDE10. Hypothetically, the (OE1) carbonyl oxygen of Gln812 could accept a hydrogen bond from the exocyclic amino group of the adenine of cAMP by rotating its side chain (Figure 8). However, this hypothesis is not supported by the fact that the Gln812Ile mutation retains full activity toward cAMP, and the IC_{50} value for EHNA is unchanged (Tables 3B and 4). Taking into account that PDE10A possesses a valine at this position and a 27-fold higher affinity for cAMP, we conclude that Gln812 does not directly take part in EHNA binding, although Gln812 might play an important role in binding the cGMP substrate.

The second important mutation is Ile826Val. It leads to a 7-fold increased IC_{50} value for EHNA compared to wild-type PDE2A (Table 4). As for the interaction with rolipram, Ile826 is positioned below the purine ring of EHNA and thereby limits the space for EHNA. Since EHNA resembles the substrate cAMP, a comparison of the enzymatic activities of mutant Ile826Val toward substrates cAMP and cGMP might elucidate the increased IC_{50} change for EHNA. The Ile826Val mutant exhibits decreased activity toward cAMP compared to the wild-type enzyme, and it is the only mutant with higher activity toward substrate cGMP (Table 3B). Substitution with a smaller valine could increase the space for inhibitor EHNA and cause the loss of hydrogen bonding with residues in the upper binding pocket, while improving hydrogen bonding with the lower binding pocket. This shift in interactions could destabilize binding of the adenine ring of EHNA, accounting for the higher IC_{50} value. Furthermore, the crystal structure of PDE4 in complex with the nonspecific inhibitor 3-isobutyl-1-methylxanthine (IBMX) shows that the equivalent residue in PDE4 (Ile336) is in close contact to the xanthine ring of IBMX and is one of several other residues that define the subpocket of PDE4 (*37*). We think that Ile826 may therefore sterically position the ligand in the active site. Alternatively, a smaller residue at this position could also induce a conformational change with neighboring residues, e.g., Tyr655 and Tyr827. These residues may encroach on the active site of PDE2A and thereby limit the access of substrate and inhibitor in the upper binding pocket.

CONCLUSIONS

The ability to rapidly produce and identify enzymatically active proteins makes the wheat germ IVT system a powerful tool for structure−activity analyses of enzymes. This inexpensive and simple system combines the advantages of rapid generation of multiple protein variants by PCR and the parallel expression and affinity capture of these proteins for functional characterizations.

The mutations reported here provide a rational explanation for the potent inhibition of PDE2A by EHNA, and the inefficacy of rolipram, as well as insights into the dual substrate specificity of PDE2A enzymes. The 200-fold greater difference in potency of EHNA and rolipram for inhibition of PDE2A can be ascribed to the steric constraints of the lower binding pocket and polar characteristics of the upper binding pocket of PDE2A, a less fitting environment for rolipram in PDE2A.

In summary, our mutational and structural studies suggest that the inhibitor specificity and selectivity determinants of PDE2A are closely linked to the shape and hydrophobicity of two patches of residues within the substrate binding pocket.

ACKNOWLEDGMENT

We thank Mrs. Jiansu Zhang for assistance with the activity screening assay and Kelvin Lam, Jason Hughes, Jason Johnson, Christine Loh, Norm Garceau, Jayvardhan Pandit, Felix Vajdos, Nickolay Chirgadze, and Steve Faraci for useful discussions and technical support.

REFERENCES

1. Houslay, M. D., and Milligan, G. (1997) Tailoring cAMP-signalling responses through isoform multiplicity, *Trends Biochem. Sci. 22*, 217−24.
2. Houslay, M. D., Sullivan, M., and Bolger, G. B. (1998) The multienzyme PDE4 cyclic adenosine monophosphate-specific phosphodiesterase family: intracellular targeting, regulation, and selective inhibition by compounds exerting anti-inflammatory and antidepressant actions, *Adv. Pharmacol. 44*, 225−342.
3. Beavo, J. A. (1995) Cyclic nucleotide phosphodiesterases: functional implications of multiple isoforms, *Physiol. Rev. 75*, 725−48.
4. Conti, M. (2000) Phosphodiesterases and cyclic nucleotide signaling in endocrine cells, *Mol. Endocrinol. 14*, 1317−27.
5. Charbonneau, H., Beier, N., Walsh, K. A., and Beavo, J. A. (1986) Identification of a conserved domain among cyclic nucleotide phosphodiesterases from diverse species, *Proc. Natl. Acad. Sci. U.S.A. 83*, 9308−12.
6. Francis, S. H., Colbran, J. L., McAllister-Lucas, L. M., and Corbin, J. D. (1994) Zinc interactions and conserved motifs of the cGMP-binding cGMP-specific phosphodiesterase suggest that it is a zinc hydrolase, *J. Biol. Chem. 269*, 22477−80.
7. Manganiello, V. C., Murata, T., Taira, M., Belfrage, P., and Degerman, E. (1995) Diversity in cyclic nucleotide phosphodiesterase isoenzyme families, *Arch. Biochem. Biophys. 322*, 1−13.
8. Corbin, J. D., Francis, S. H., and Webb, D. J. (2002) Phosphodiesterase type 5 as a pharmacologic target in erectile dysfunction, *Urology 60*, 4−11.
9. Rosen, R. C., and Kostis, J. B. (2003) Overview of phosphodiesterase 5 inhibition in erectile dysfunction, *Am. J. Cardiol. 92*, 9M−18M.
10. Rosman, G. J., Martins, T. J., Sonnenburg, W. K., Beavo, J. A., Ferguson, K., and Loughney, K. (1997) Isolation and characterization of human cDNAs encoding a cGMP-stimulated 3′,5′-cyclic nucleotide phosphodiesterase, *Gene 191*, 89−95.
11. Martinez, S. E., Wu, A. Y., Glavas, N. A., Tang, X. B., Turley, S., Hol, W. G., and Beavo, J. A. (2002) The two GAF domains in phosphodiesterase 2A have distinct roles in dimerization and in cGMP binding, *Proc. Natl. Acad. Sci. U.S.A. 99*, 13260−5.
12. Aravind, L., and Ponting, C. P. (1997) The GAF domain: an evolutionary link between diverse phototransducing proteins, *Trends Biochem. Sci. 22*, 458−9.
13. Torphy, T. J., Stadel, J. M., Burman, M., Cieslinski, L. B., McLaughlin, M. M., White, J. R., and Livi, G. P. (1992) Coexpression of human cAMP-specific phosphodiesterase activity and high affinity rolipram binding in yeast, *J. Biol. Chem. 267*, 1798−804.
14. Hayashi, M., Matsushima, K., Ohashi, H., Tsunoda, H., Murase, S., Kawarada, Y., and Tanaka, T. (1998) Molecular cloning and characterization of human PDE8B, a novel thyroid-specific isozyme of 3′,5′-cyclic nucleotide phosphodiesterase, *Biochem. Biophys. Res. Commun. 250*, 751−6.
15. Hetman, J. M., Soderling, S. H., Glavas, N. A., and Beavo, J. A. (2000) Cloning and characterization of PDE7B, a cAMP-specific phosphodiesterase, *Proc. Natl. Acad. Sci. U.S.A. 97*, 472−6.
16. Soderling, S. H., Bayuga, S. J., and Beavo, J. A. (1998) Cloning and characterization of a cAMP-specific cyclic nucleotide phosphodiesterase, *Proc. Natl. Acad. Sci. U.S.A. 95*, 8991−6.
17. Fisher, D. A., Smith, J. F., Pillar, J. S., St Denis, S. H., and Cheng, J. B. (1998) Isolation and characterization of PDE9A, a novel human cGMP-specific phosphodiesterase, *J. Biol. Chem. 273*, 15559−64.
18. Hetman, J. M., Robas, N., Baxendale, R., Fidock, M., Phillips, S. C., Soderling, S. H., and Beavo, J. A. (2000) Cloning and characterization of two splice variants of human phosphodiesterase 11A, *Proc. Natl. Acad. Sci. U.S.A. 97*, 12891−5.
19. MacFarland, R. T., Zelus, B. D., and Beavo, J. A. (1991) High concentrations of a cGMP-stimulated phosphodiesterase mediate ANP-induced decreases in cAMP and steroidogenesis in adrenal glomerulosa cells, *J. Biol. Chem. 266*, 136−42.
20. Huai, Q., Wang, H., Sun, Y., Kim, H. Y., Liu, Y., and Ke, H. (2003) Three-dimensional structures of PDE4D in complex with roliprams and implication on inhibitor selectivity, *Structure (Cambridge, MA, U.S.) 11*, 865−73.
21. Schilling, R. J., Morgan, D. R., and Kilpatrick, B. F. (1994) A high-throughput assay for cyclic nucleotide phosphodiesterases, *Anal. Biochem. 216*, 154−8.
22. Bradford, M. M. (1976) A rapid and sensitive method for the quantitation of microgram quantities of protein utilizing the principle of protein-dye binding, *Anal. Biochem. 72*, 248−54.
23. Kozak, M. (1991) Effects of long 5′ leader sequences on initiation by eukaryotic ribosomes in vitro, *Gene Expression 1*, 117−25.
24. Kozak, M. (1988) Leader length and secondary structure modulate mRNA function under conditions of stress, *Mol. Cell. Biol. 8*, 2737−44.
25. Johnson, J. D., Walters, J. D., and Mills, J. S. (1987) A continuous fluorescence assay for cyclic nucleotide phosphodiesterase hydrolysis of cyclic GMP, *Anal. Biochem. 162*, 291−5.
26. Otwinowski, Z., and Minor, W. (1997) Processing of X-Ray Diffraction Data Collected in Oscillation Mode, *Methods Enzymol. 276*, 307−26.
27. Kissinger, C. R., Gehlhaar, D. K., and Fogel, D. B. (1999) Rapid automated molecular replacement by evolutionary search, *Acta Crystallogr., Sect. D: Biol. Crystallogr. 55 (Part 2)*, 484−91.
28. Xu, R. X., Hassell, A. M., Vanderwall, D., Lambert, M. H., Holmes, W. D., Luther, M. A., Rocque, W. J., Milburn, M. V., Zhao, Y., Ke, H., and Nolte, R. T. (2000) Atomic structure of PDE4: insights into phosphodiesterase mechanism and specificity, *Science 288*, 1822−5.
29. Murshudov, G. N., Vagin, A. A., Lebedev, A., Wilson, K. S., and Dodson, E. J. (1999) Efficient anisotropic refinement of macromolecular structures using FFT, *Acta Crystallogr., Sect. D: Biol. Crystallogr. 55* (*Part 1*), 247−55.
30. Jones, T. A., Zou, J. Y., Cowan, S. W., and Kjeldgaard (1991) Improved methods for building protein models in electron density maps and the location of errors in these models, *Acta Crystallogr., Sect. A 47* (*Part 2*), 110−9.
31. Huai, Q., Colicelli, J., and Ke, H. (2003) The crystal structure of AMP-bound PDE4 suggests a mechanism for phosphodiesterase catalysis, *Biochemistry 42*, 13220−6.
32. Mumby, M. C., Martins, T. J., Chang, M. L., and Beavo, J. A. (1982) Identification of cGMP-stimulated cyclic nucleotide phosphodiesterase in lung tissue with monoclonal antibodies, *J. Biol. Chem. 257*, 13283−90.
33. Essayan, D. M. (1999) Cyclic nucleotide phosphodiesterase (PDE) inhibitors and immunomodulation, *Biochem. Pharmacol. 57*, 965−73.

34. Zhang, K. Y., Card, G. L., Suzuki, Y., Artis, D. R., Fong, D., Gillette, S., Hsieh, D., Neiman, J., West, B. L., Zhang, C., Milburn, M. V., Kim, S. H., Schlessinger, J., and Bollag, G. (2004) A Glutamine Switch Mechanism for Nucleotide Selectivity by Phosphodiesterases, *Mol. Cell 15*, 279−86.
35. Scapin, G., Patel, S. B., Chung, C., Varnerin, J. P., Edmondson, S. D., Mastracchio, A., Parmee, E. R., Singh, S. B., Becker, J. W., Van der Ploeg, L. H., and Tota, M. R. (2004) Crystal structure of human phosphodiesterase 3B: atomic basis for substrate and inhibitor specificity, *Biochemistry 43*, 6091−100.
36. Huai, Q., Wang, H., Zhang, W., Colman, R. W., Robinson, H., and Ke, H. (2004) Crystal structure of phosphodiesterase 9 shows orientation variation of inhibitor 3-isobutyl-1-methylxanthine binding, *Proc. Natl. Acad. Sci. U.S.A. 101*, 9624−9.
37. Huai, Q., Liu, Y., Francis, S. H., Corbin, J. D., and Ke, H. (2004) Crystal structures of phosphodiesterases 4 and 5 in complex with inhibitor 3-isobutyl-1-methylxanthine suggest a conformation determinant of inhibitor selectivity, *J. Biol. Chem. 279*, 13095−101.
38. Card, G. L., England, B. P., Suzuki, Y., Fong, D., Powell, B., Lee, B., Luu, C., Tabrizizad, M., Gillette, S., Ibrahim, P. N., Artis, D. R., Bollag, G., Milburn, M. V., Kim, S. H., Schlessinger, J., and Zhang, K. Y. (2004) Structural basis for the activity of drugs that inhibit phosphodiesterases, *Structure (Cambridge, MA, U.S.) 12*, 2233−47.
39. Xu, R. X., Rocque, W. J., Lambert, M. H., Vanderwall, D. E., Luther, M. A., and Nolte, R. T. (2004) Crystal structures of the catalytic domain of phosphodiesterase 4B complexed with AMP, 8-Br-AMP, and rolipram, *J. Mol. Biol. 337*, 355−65.
40. Fujishige, K., Kotera, J., Michibata, H., Yuasa, K., Takebayashi, S., Okumura, K., and Omori, K. (1999) Cloning and characterization of a novel human phosphodiesterase that hydrolyzes both cAMP and cGMP (PDE10A), *J. Biol. Chem. 274*, 18438−45.
41. Soderling, S. H., Bayuga, S. J., and Beavo, J. A. (1999) Isolation and characterization of a dual-substrate phosphodiesterase gene family: PDE10A, *Proc. Natl. Acad. Sci. U.S.A. 96*, 7071−6.
42. Richter, W., Unciuleac, L., Hermsdorf, T., Kronbach, T., and Dettmer, D. (2001) Identification of inhibitor binding sites of the cAMP-specific phosphodiesterase 4, *Cell. Signalling 13*, 287−97.
43. Richter, W., Unciuleac, L., Hermsdorf, T., Kronbach, T., and Dettmer, D. (2001) Identification of substrate specificity determinants in human cAMP-specific phosphodiesterase 4A by single-point mutagenesis, *Cell. Signalling 13*, 159−67.
44. Card, G. L., Blasdel, L., England, B. P., Zhang, C., Suzuki, Y., Gillette, S., Fong, D., Ibrahim, P. N., Artis, D. R., Bollag, G., Milburn, M. V., Kim, S. H., Schlessinger, J., and Zhang, K. Y. (2005) A family of phosphodiesterase inhibitors discovered by cocrystallography and scaffold-based drug design, *Nat. Biotechnol. 23*, 201−7.

BI047313H